Dalton Transactions

Accepted Manuscript

ROYAL SOCIETY OF CHEMISTRY

www.rsc.org/dalton

Journal Name

PAPER

Characterization of modified SiC@SiO_2 nanocables/MnO_2 and their potential application as hybrid electrodes for supercapacitors

Received 00th January 20xx,
Accepted 00th January 20xx

DOI: 10.1039/x0xx00000x

www.rsc.org/

Yujie Zhang[a], Junhong Chen[b*], Huili Fan[a], Kuo-Chih Chou[c] and Xinmei Hou[c*]

In this research, we demonstrate a simple route for preparing SiC@SiO_2 core-shell nanocables and further obtain SiC@SiO_2 nanocables/MnO_2 as hybrid electrodes for supercapacitors using various modified methods. The modified procedure consists of mildly modifications by sodium hydroxide as well as UV light irradiation and deposition of MnO_2. The morphology and microstructural characteristics of the composites are investigated by XRD, XPS, FE-SEM with EDS and TEM. The results indicate that the surfaces of modified SiC@SiO_2 nanocables are equably coated with MnO_2 thin layer. The electrochemical behaviors of the hybrid electrodes are systematically measured in a three-electrode system using cyclic voltammetry, galvanostatic charge/discharge and electrochemical impedance spectroscopy. The as-resultant electrode presents a superb charge storage characteristic with large specific capacitance of 276.3 F g^{-1} at the current density of 0.2 A g^{-1}. Moreover, the hybrid electrode also displays a long circle life with a good capacitance retention (~92.0%) after 1000 CV cycles, exhibiting promising potential for supercapacitors.

1. Introduction

The fast-growing alternative energy storage demand in applications, ranging from portable electronic devices and consumer electronics to hybrid electric vehicles and large industrial equipment, has been of the world-wide considerable interest, due to up-coming depletion of fossil fuels and ever-increasing environmental problems.[1,2] Of the various power source devices, supercapacitors storing energy through either ion adsorption (electrochemical double-layer capacitor, EDLC) or fast surface redox reactions (pseudocapacitor), has been an attractive power solution because of their distinguished properties such as high power density, fast charge-discharge rate, noticeable power output, long cycle life and remarkable reliability.[3-6] In EDLCs, no chemical reaction happens and only adsorption/desorption of electrolyte ions on the surface of active materials occur during the charge/discharge process. Up to now, such systems as high specific surface carbon[7-10], semiconductor with nanostructure for instance, silicon nanowires, silicon carbide (SiC) nanowires, titanium dioxide (TiO_2) nanotubes/nanowires and titanium nitride (TiN) nanowires[11-16] are adopted as EDLCs. Among these, 3C-SiC exerts a tremendous fascination on investigators because 3C-SiC possesses the smallest band gap (~2.4 eV), the largest electron mobilities (~800 cm^2 V^{-1} s^{-1} in a low-doped material) and excellent electronic conductivity of all SiC polytypes.[17] In pseudo capacitors, reversible redox reactions occur during the charge/discharge process. Usually metal oxides and conducting polymers are applied as pseudo capacitors.[18-25] Among all the active materials for pseudo capacitors, MnO_2 has received extensive attention due to its abundance in nature, low cost, its high theoretical specific capacitance and environmentally benign characters. However, essential improvement in performance still remains a huge challenge for supercapacitors to gain more dramatical properties in the future.[26] Therefore it is of far-reaching significance to explore various material systems used for supercapacitors.

Currently developing composite materials combining EDLC and pseudo capacitance as hybrid electrodes for supercapacitors have been given rise to the enthusiasm of researchers. Zhang *et al.* pointed out that the specific capacitance of the activated carbon electrode can be notably improved by incorporating birnessite-type MnO_2.[27] Cheng *et al.* fabricated MnO_2/activated-carbon-paper through an electrodeposition route. The electrode showed a specific capacitance of 757.0 F g^{-1} at a scan rate of 10 mV s^{-1}.[4] SiC nanowires grown on carbon fabric demonstrated high areal capacitances of 23 mF cm^{-2} at a scan rate of 50 mV s^{-1}, long cycle lives and good flexible properties.[28] Kim *et al.* adopted microsphere SiC/nanoneedle manganese oxide composites as macrosupercapacitor electrodes with the specific capacitance of 251.3 F g^{-1} at a scan rate of 10 mV s^{-1}.[29] To further improve the performance of capacitor electrodes, Sha's work group investigated SiC nanowires@$Ni(OH)_2$ core-shell

[a] School of Chemistry and Biological Engineering, University of Science & Technology Beijing, Beijing 100083, China
[b] School of Material Science and Engineering, University of Science & Technology Beijing, Beijing 100083, China. E-mail: cjh@ustb.edu.cn. Tel: +86 10 62332666 (J.C.).
[c] State Key Laboratory of Advanced Metallurgy, University of Science &Technology Beijing, Beijing 100083, China. E-mail: houxinmei@ustb.edu.cn; Fax: +86 10 6233 3622; Tel: +86 10 6233 3622.

structures on carbon fabric for supercapacitor electrodes and showed excellent specific capacitance of 1724 F g^{-1} at 2 A g^{-1}.[30]

In this work, large-scale 3C-SiC@SiO_2nanocables with core-shell structure were synthesized using a simple route.[31] Several methods to modify the surface of SiC@SiO_2 nanocables including etching by sodium hydroxide (NaOH) and photo-induced conversion (UV illumination) were adopted. Based on this, MnO_2 was deposited on the surface of treated SiC@SiO_2 core-shell nanocables. Thereby modified SiC@SiO_2 nanocables/MnO_2composites were prepared aiming to be applied as hybrid electrodes for supercapacitors with improved electrochemical properties.

2. Experimental

2.1 Material preparation

SiO_2@SiC nanocables were prepared by a simple and low-cost synthesis route using gangue (SiO_2>99%) and carbon black as raw material. It was prepared at 1500°C for 2h at argon atmosphere. The preparation procedure is similar to SiC whikers synthesis reported in our previous work.[31] For simplification, SiC@SiO_2 core-shell nanocables are denoted as SiC@SiO_2.

Several methods were adopted to modify the surface of SiC@SiO_2. One method is combing etching by NaOH with UV irradiation. It is well known that photo-induced including UV conversion as a way of surface modification is extraordinarily attractive.[32] Some researchers demonstrated that UV light could improve the hydrophilic property and surfactivity.[33,34] This could contribute significantly to adsorb electrical charge to form electric double layer with the electrolyte. Therefore UV light is adopted in this work. The procedure is as following: 0.5 g of SiC@SiO_2 nanocables was dispersed in 1 mol L^{-1} NaOH solution (40 ml) and magnetically stirred for 1 h at 70 °C. Then the mixture was filtered with distilled water until the pH of the resulting water was between 7-8. The obtained whiskers were dried at 80 °C for 12 h. Finally the above obtained samples were exposed to UV irradiation for 1 h at ambient temperature (20 °C) with the humidity of 39 %. The UV light was generated by a 500-W high-pressure Hg lamp with a filter centered at 254 nm. The obtained sample was symbolized as SiC@SiO_2 (NaOH+UV).

The second method is depositing MnO_2 on the surface of SiC@SiO_2 nanocables. The procedure is as follows: SiC@SiO_2 (NaOH+UV) and $KMnO_4$ with the mole ratio of 1:1 were dissolved in moderate deionized water to form a precursor solution. Then the mixture was equably stirred in thermostatic oil bath and refluxed at 120 °C for 10 h. The resultant products were filtered and centrifuged several times with deionized water until the purple color of the solution disappeared. Then the sample was dried at 80 °C in air for 12 h. The obtained sample was symbolized as SiC@SiO_2 (NaOH+UV)/MnO_2. For comparison, part of SiC@SiO_2 was firstly etched by NaOH solution and then was directly dissolved in $KMnO_4$ without UV irradiation to obtain SiC@SiO_2 nanocables/MnO_2 composites. The obtained sample was named as SiC@SiO_2 (NaOH)/MnO_2. For comparison, a control experiment to obtain pure MnO_2 was carried out by the reaction between $KMnO_4$ and hydrochloric acid.

2.2 Preparation of supercapacitor electrode

The work electrode was prepared by mixing the above sample, i.e. SiC@SiO_2, SiC@SiO_2 (NaOH+UV), SiC@SiO_2 (NaOH+UV)/MnO_2, SiC@SiO_2 (NaOH)/MnO_2 or MnO_2, acetylene black and polyvinylidene fluoride (PVDF) with the mass ratio of 7:2:1 in N-methyl-2-pyrrolidone (NMP) and the stable slurry was coated on a Ti sheet with the coating area of 1×1cm. The electrode was heated at 80 °C for 24 h to evaporate the solvent.

2.3 Material characterizations

X-ray diffraction (XRD) patterns of the samples were obtained on PW-1830 X-ray diffractometer (Philips) with Cu Kα from 5°to 80°(2θ) with a scanning speed of 1°/min. X-ray photoelectron spectroscopy (XPS) measurements were performed on ESCALAB 250Xi (Thermo Fisher Scientific). The morphology of the prepared samples was examined using field-emission scanning electron microscopy (FE-SEM, FEI-SIRION, operated at 5 kV) and transmission electron microscopy (TEM) (Tecnai G2 F30 S-TWIN). The specific surface area was determined from the nitrogen adsorption-desorption isotherm measured at -196 °C on a Quadrasorb SI-MP analyzer using Brunauer-Emmett-Teller (BET) model. The measurements of contact angles of samples were measured on a piece of Marcellus shale using a DSA100 instrument (Kruss) at room temperature.

The electrochemical behaviors were investigated on a CHI660E electrochemistry working station. A three-electrode system was adopted and the auxiliary and reference electrode were platinum foil and Ag/AgCl (KCl-saturated) respectively. The electrolyte used in all of the measurements was 1 M Na_2SO_4 aqueous solution. Cyclic voltammetry (CV), galvanostatic charge/discharge characteristics and electrochemical impedance spectroscopy (EIS) were carried out. The potential range for CV tests was −0.1 to +0.9 V and the scan rates were in the range of 5 to 100 mV s^{-1}. Galvanostatic charge/discharge measurements were carried out from −0.1 to +0.9 V with different current densities at 0.2, 0.5, 1 and 2 A g^{-1}. EIS measurements were done by applying an AC voltage with 5 mV amplitude in a frequency range from 0.1 Hz to 100 kHz.

3. Results and discussion

3.1 Morphology and structure characterization

Figure 1 is the photograph of the synthesized SiC@SiO_2 nanocables. It shows that the nanocables are considerably lightweight that they can stand on the clover (Figure 1a). Besides, SiC@SiO_2 nanocables exhibit good flexibility similar to cotton (Figure 1b).

As for the phases of SiC@SiO_2 nanocables after modification, XRD patterns are shown in Fig.2. Fig.2a is XRD patterns of SiC@SiO_2, SiC@SiO_2 (NaOH+UV) and SiC@SiO_2 (NaOH+UV)/MnO_2. For SiC@SiO_2, the broad peak at about 22° corresponds to the amorphous SiO_2 shells. The other five reflection peaks from 30 to 80° can be indexed to be cubic SiC (Card NO. 01-073-1706). It shows that SiO_2@SiC nanocables are synthesized using this simple method. In view of SiC@SiO_2 (NaOH+UV), it can be seen that the characteristic peaks of 3C-SiC remain after NaOH treatment. By

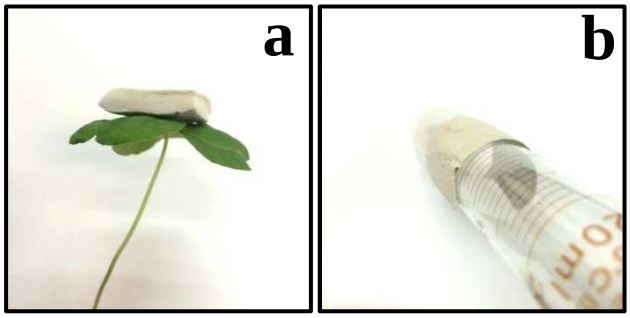

Fig.1 (a) Photograph of the as-received SiC@SiO_2 nanocables standing on the clover; (b) the as-received SiC@SiO_2 nanocables on a test tube.

comparison, the relative intensity of the broad peak at about 22° corresponding to amorphous silica is obviously weakened, indicating most of silica is mildly removed by NaOH. In nature, the surfaces of SiC whiskers would be apt to form stable SiO_2 thin layer via adsorbing oxygen even at room temperature.[35] In this work, an ultrathin layer of SiO_2 was reserved via controlling the moderate treatment condition aiming to increase the stability of core SiC whiskers and boost the surfactivity of shell SiO_2. After treated by $KMnO_4$, a new broad peak at about 12° appears as shown in SiC@SiO_2 (NaOH+UV)/MnO_2, which corresponds to (0 0 1) of δ-MnO_2. Besides this, the characteristic peaks of SiC remains and no signal of SiO_2 is found, which is possibly caused by the deposition of MnO_2 on the surface and thus suppresses the intensity of silica. Further investigation is carried out in the following section.

The detailed surface information is collected using XPS as shown in Figs.2b-f. It can be seen from Fig.2b that both SiC@SiO_2 and SiC@SiO_2 (NaOH+UV) consist of Si, O and C. By comparison, the relative density of O 1s signal decreases in SiC@SiO_2 (NaOH+UV), indicating that oxygen atoms existing as SiO_2 are gently removed by NaOH. In view of SiC@SiO_2 (NaOH+UV)/MnO_2, Mn signal ($2p_{3/2}$, $2p_{1/2}$) is observed besides Si, O and C, indicating that MnO_2 is probably deposited on the surface of SiC@SiO_2 nanocables. The relative intensity of Si and C peak decreases clearly owing to the uniform adhesion of MnO_2 on the surface. The valence of manganese is considerably vital when manganese oxide is used as the supercapacitor cathode. To acquire the detailed surface information, the manganese oxidation state in SiC@SiO_2 (NaOH+UV)/MnO_2 is investigated using XPS spectroscopic data for O 1s, Mn 2p and Mn 3s (as shown in Fig.2c-f). During redox switching, the change of manganese oxidation state can be confirmed by O 1s core-level spectrum.[36,37] O 1s core-level spectra (Fig.2c) of SiC@SiO_2 indicate the only strong SiO_2 peak at 532.84 eV.[38] In contrast, O 1s core-level spectra of SiC@SiO_2 (NaOH+UV)/MnO_2 exhibit three kinds of oxygen bonds, i.e. water (H−O−H) and low concentrations of SiO_xC_y at 532.9 eV,[29,39] Mn-O-H peak at 531.2 eV and Mn-O-Mn peak at 529.9 eV as shown in Fig. 2d.[29,40] In addition, the average oxidation state of manganese can be obtained by calculating the area of the peaks associated with Mn-O-Mn and Mn-O-H using the following formula: [36]

$$\text{manganese oxidation state} = [\text{IV} \cdot (S_{\text{Mn-O-Mn}} - S_{\text{Mn-O-H}}) + \text{III} \cdot S_{\text{Mn-O-H}}]/S_{\text{Mn-O-Mn}}$$

where S stands for the signal of the different components of O 1s spectrum. As shown in Fig. 2e, the relative peak areas of Mn-O-Mn and Mn-O-H are 69.94, 13.77% respectively. Therefore the average oxidation state of manganese in the as-synthesized MnO_2 of the composite is 3.8, indicating the as-prepared manganese oxidation in the composites is mainly composed of tetravalent systems. In addition, two peaks at 642.2 eV and 653.9 eV corresponding to the binding energies of Mn $2p_{3/2}$ and Mn $2p_{1/2}$ are observed in Fig.2e. The spin-energy separation between Mn $2p_{3/2}$ and Mn $2p_{1/2}$ peaks is 11.7 eV, indicating the presence of tetravalent Mn. This also agrees well with the results previously reported for MnO_2.[41] However it is inadequate to determine the accurate manganese oxidation state only from Mn 2p spectrum due to either the broadening or tailing of peaks at lower binding energy.[42] More pivotal information can be obtained by analysis of Mn 3s spectra which manifests a peak splitting and a doublet because a parallel spin couples between 3s and 3d electron in time of the photoelectron ejection. [39,42] A peak splitting of Mn 3s core-level spectrum is observed in Fig.2f. The peak energy separation (ΔE) is 4.81 eV. According to the analogously linear relationship between ΔE and the oxidation state of Mn reported by Toupin*et.al*,[42] the average oxidation state of manganese is 3.8, which is in consistent with the above experimental result.

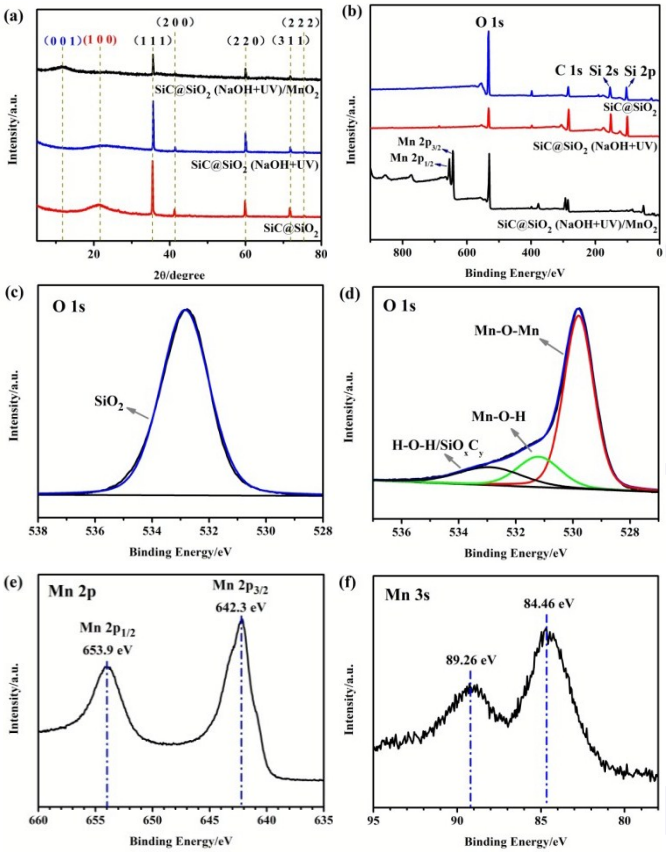

Fig. 2 (a) XRD patterns of SiC@SiO_2, SiC@SiO_2 (NaOH+UV) and SiC@SiO_2 (NaOH+UV)/MnO_2; (b) XPS wide scan survey spectra of SiC@SiO_2, SiC@SiO_2 (NaOH+UV) and SiC@SiO_2 (NaOH+UV)/MnO_2; (c) XPS spectra of O 1s peaks of SiC@SiO_2; (d) XPS spectra of O 1s peaks of SiC@SiO_2 (NaOH+UV)/MnO_2; (e) XPS spectra of Mn 2p peaks of SiC@SiO_2 (NaOH+UV)/MnO_2; (f) XPS spectra of Mn 3s peaks of SiC@SiO_2 (NaOH+UV)/MnO_2.

The morphology of the obtained SiC@SiO_2, SiC@SiO_2

(NaOH+UV) and $SiC@SiO_2$ (NaOH+UV)/MnO_2 is further characterized using

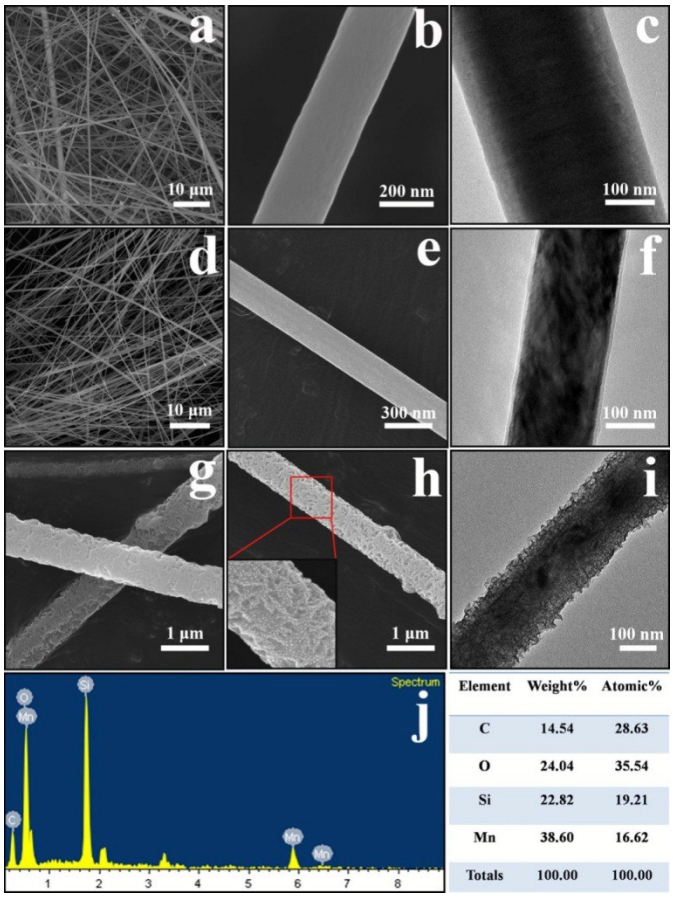

Fig.3 (a, b) FE-SEM images of the as-prepared $SiC@SiO_2$ at low and high magnifications, respectively; (d, e) FE-SEM images of $SiC@SiO_2$ (NaOH+UV) at low and high magnifications respectively; (g, h) FE-SEM images of $SiC@SiO_2$ (NaOH+UV)/MnO_2, and the inset in (h) is the magnified FE-SEM image of the region marked by the red rectangle; (j) EDS of the marked region in (h); (c, f, i) TEM images of $SiC@SiO_2$, $SiC@SiO_2$ (NaOH+UV) and $SiC@SiO_2$ (NaOH+UV)/MnO_2.

FE-SEM and TEM analysis. The images of the as-received $SiC@SiO_2$ nanocables at low and high magnification (shown in Figs.3a and b) indicate the majority of $SiC@SiO_2$ nanocables can be described as straight and long filaments possessing smooth surface with diameters ranging from 100 to 500 nm. The shell of SiO_2 can be clearly observed by TEM with the thickness of about 30 nm (Fig.3c). After etching by NaOH solution and UV illumination, the surface becomes a little coarser as shown in Figs.3d and e. TEM analysis indicates that the thickness of SiO_2 becomes extremely thin, i.e. approximately 3~8 nm (Fig.3f). As for the morphology of $SiC@SiO_2$ (NaOH+UV)/MnO_2, it can be seen that the surfaces became extremely rough and rugged with multiholes (Fig.3g-i). Moreover, there is an obvious boundary between inner spindle and outer layer (Fig.3i). EDS result (Fig.3j) of the marked region in Fig. 3h reveals that the as-received composites contain elements of C, O, Si and Mn. This phenomenon is in agreement with the results of XRD and XPS analysis. To further investigate the existence of multiholes, TEM analysis was carried out as shown in Figs. 4a and b. Many mesopores existed marked by red circles. In addition, the surface was very rough. By comparison, the morphology of pure MnO_2 particles is also investigated. It can be seen that the surface is also rough and consists of many mesopores (Figs.4c and d). The nitrogen adsorption and desorption isotherms of $SiC@SiO_2$ (NaOH+UV)/MnO_2 are given in Fig.5. The results illustrate the specific surface area of the composite is about 527 m^2 g^{-1} and the mesopores primarily range from 2 to 4 nm. The mesopores and rough surface contribute to the big surface area of the sample.

The homogeneous deposition is attributed to mildly treatment of silica layer on the surfaces of $SiC@SiO_2$ nanocables with high specific surface area and mesopores for energy storage. As a result, it brings about not only the hydrated ions in electrolyte close to the exterior and interior pore surfaces, but also the shorter transport/diffusion channel lengths for both ions and electrons, which thus improves both the main pseudo capacitance of MnO_2 and the electric double-layer capacitance (EDLC) of $SiC@SiO_2$ nanocables.[29,43]

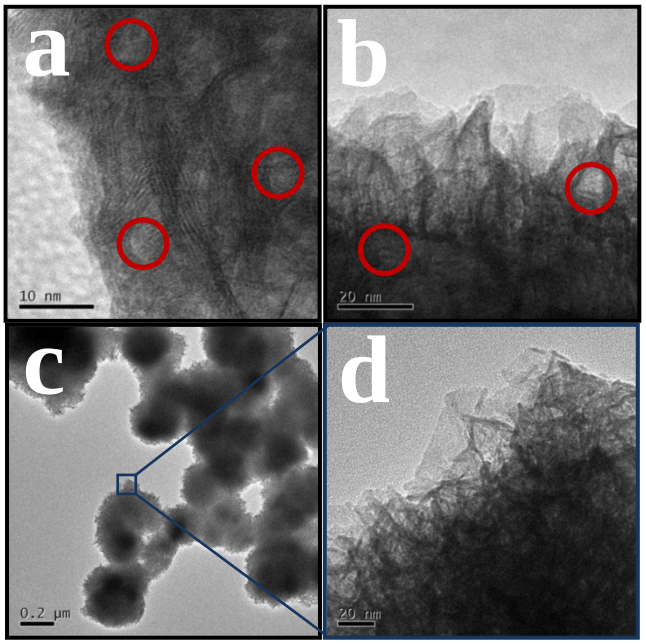

Fig. 4 (a,b) HRTEM images of $SiC@SiO_2$ (NaOH+UV)/MnO_2; (c) TEM image of pure MnO_2;(d) The magnified TEM image of the region marked by the dark-blue rectangle in (c).

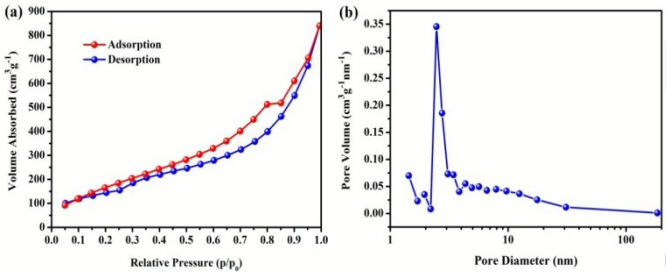

Fig. 5 (a) Nitrogen adsorption-desorption isotherm and (b) pore size distribution of $SiC@SiO_2$ (NaOH+UV)/MnO_2

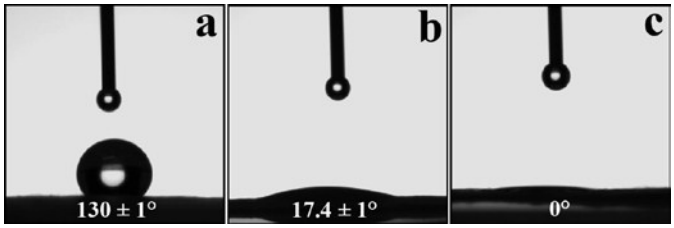

Fig. 6 Water contact angles of $SiC@SiO_2$, $SiC@SiO_2$ (NaOH+UV) and $SiC@SiO_2$ (NaOH+UV)/MnO_2.

The hydrophobic property of the samples was measured by using a contact angle instrument (Fig.6). It can be seen that $SiC@SiO_2$ nanocables is superhydrophobic with a contact angle (CA) of about 130 ± 1° in Fig. 6a. After modification by NaOH and UV, the CA of $SiC@SiO_2$ (NaOH+UV) is approximately 17.4 ± 1° (Fig.6b), indicating the hydrophily of modified $SiC@SiO_2$nanocables is greatly improved. The CA of $SiC@SiO_2$ (NaOH+UV)/MnO_2 is close to 0° demonstrating that the hybrid materials possess good hydrophily (Fig.6c). The main reason is possibly that the porous and coarse surfaces are produced by modification as shown in Figs. 3 and 4.

3.2 Electrochemical capacitive performance

Figure 7a shows a comparison of the CV curves of $SiC@SiO_2$, $SiC@SiO_2$ (NaOH+UV), $SiC@SiO_2$ (NaOH+UV)/MnO_2, $SiC@SiO_2$ (NaOH) and MnO_2 electrodes at a scan rate of 10mV s^{-1} with potential windows ranging from −0.1 to +0.9 V in 1 M Na_2SO_4 electrolyte. Obviously, the CV plots are close to rectangular shape and a mirror-image feature, exhibiting excellent reversibility and ideal capacitive behavior.[29,44] As shown by FE-SEM images, $SiC@SiO_2$ with long and straight filaments structure possess an excellent electronic conductivity because β-SiC exhibits the smallest band gap (~2.4 eV) and the largest electron mobilities (~800 cm^2 V^{-1} s^{-1} in a low-doped material) of all SiC polytypes.[17] Therefore the capacitive characteristics of $SiC@SiO_2$ as electrode are ascribed to the excellent electrical conductivity, electric double-layer capacity and electroactive areas. After modified by NaOH and UV irradiation, the capacitive performance of $SiC@SiO_2$ (NaOH+UV) has been improved to some extent while with no obvious change. While the capacitive behavior of $SiC@SiO_2$ (NaOH+UV)/MnO_2 is noticeably promoted owing to the following reasons. First, MnO_2 is homogeneous deposited on the surface; Second, UV irradiation can boost the hydrophilic property and surfactivity of the surface, which could lead to the better capacitive property.[33,34] This could contribute significantly to adsorb electrical charge to form electric double layer with the electrolyte. For comparison, the CV curve of MnO_2 possesses the largest area, which reveals the remarkable pseudocapacitive behavior (Fig.7a).

In order to further survey the advantages of $SiC@SiO_2$ (NaOH+UV)/MnO_2 as supercapacitor electrodes, the CV curves of $SiC@SiO_2$ (NaOH+UV)/MnO_2 electrode over a wider range of scan rates are measured as shown in Fig. 7b. It can be seen that the current response exhibits corresponding increases with the increase of the scan rate. What's more, the CV loop of $SiC@SiO_2$ (NaOH+UV)/MnO_2 electrode yet maintains an ideal rectangular CV shape without distinct distortion at the scan rate as high as 100 mV s^{-1}.

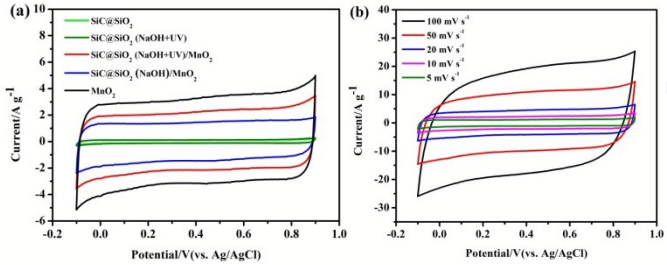

Fig. 7 (a) CV curves of $SiC@SiO_2$, $SiC@SiO_2$ (NaOH+UV), $SiC@SiO_2$ (NaOH+UV)/MnO_2, $SiC@SiO_2$ (NaOH)/MnO_2 and MnO_2 at a scan rate of 10 mV s^{-1}; (b) CV curves of $SiC@SiO_2$ (NaOH+UV)/MnO_2 electrode measured as different scan rates of 5, 10, 20, 50, and 100 mV s^{-1}.

For further evaluating the specific capability of $SiC@SiO_2$ (NaOH+UV)/MnO_2 electrodes, the galvanostatic charge/discharge curves of $SiC@SiO_2$ (NaOH+UV)/MnO_2 electrodes measured between −0.1 and +0.9 V at current densities of 0.2, 0.5, 1 and 2 A g^{-1} are shown in Fig. 8a. The charge curves are emblematically symmetric to their corresponding discharge counterparts with a slight curvature. Even when the current density increases to 2 A g^{-1}, there are low voltage losses, exhibiting low internal resistances within electrode for the directly deposition of MnO_2 onto modified $SiC@SiO_2$ nanocables and the poriferous structure of the composites electrode. The phenomenon suggests that the composite electrode exhibits an excellent capacitive performance with the co-existence of electric double layer capacitor and pseudo capacitance.[45] As we know, the specific capacitance of the electrode measured by the galvanostatic charge/discharge method can be calculated according to the following equation:[46]

$$C = \frac{I\Delta t}{\Delta V m}$$

where $C(Fg^{-1})$ is the specific capacitance, $I(A)$ is the constant discharging current, $\Delta t\ (s)$ is the discharge time, $\Delta V(V)$ is the potential window, and $m\ (g)$ is the mass of the active material in the electrode. The specific capacitances of $SiC@SiO_2$, $SiC@SiO_2$ (NaOH+UV), $SiC@SiO_2$ (NaOH+UV)/MnO_2, $SiC@SiO_2$ (NaOH)/MnO_2 and MnO_2 electrodes against the current density are plotted in Fig.8b, in which all electrodes show gradually decreased capacitance with the increase of the current density from 0.2 to 5A g^{-1}. It is clearly found from the specific capacitance curves that the specific capacitance of $SiC@SiO_2$ (NaOH+UV)/MnO_2 electrode is 276.3 F g^{-1} at the current density of 0.2 A g^{-1}. The calculated C values of $SiC@SiO_2$, $SiC@SiO_2$ (NaOH+UV), $SiC@SiO_2$ (NaOH)/MnO_2 and MnO_2 electrodes at 0.2 A g^{-1} are 15.3 F g^{-1}, 16.6 F g^{-1}, 210.2 F g^{-1} and 341.5 F g^{-1}, respectively. Relatively low as the specific capacitance of $SiC@SiO_2$ electrode is, the electrochemical capacitive performance of $SiC@SiO_2$ (NaOH+UV)/MnO_2 is enhanced with the pseudo capacitive reaction of the homogeneous deposited MnO_2. Table 1 gives the comparison of various published results of SiC-based supercapacitor electrodes.[12,13,29,47-49] In order to compare these results expediently, the resultant specific capacitances of the electrodes are transformed to another unit form. Although a little low as the specific capacitance of $SiC@SiO_2$ nanocables is, the

specific capacitance of modified SiC@SiO_2 nanocables/MnO_2 in this work is the highest between pure SiC electrodes and hybrid electrodes composed of SiC and MnO_2. Combining its simple synthesis route in this work and the properties of 3C-SiC such as the smallest band gap (~2.4 eV), the largest electron mobilities (~800 $cm^2V^{-1}s^{-1}$ in a low-doped material) and excellent electronic conductivity of all SiC polytypes, 3C-SiC can be applied as a promising hybrid electrode candidate.

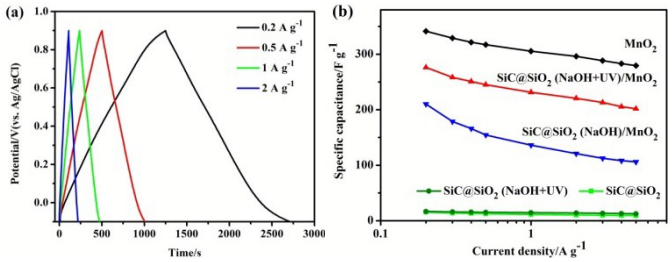

Fig. 8 (a) Galvanostatic charge/discharge curves of SiC@SiO_2 (NaOH+UV)/MnO_2 electrodes at current densities of 0.2, 0.5, 1 and 2 A g^{-1}; (b) Comparison of specific capacitances of SiC@SiO_2, SiC@SiO_2 (NaOH+UV), SiC@SiO_2 (NaOH+UV)/MnO_2, SiC@SiO_2 (NaOH)/MnO_2 and MnO_2 electrodes at different current densities.

As for the relative contribution of various factors, e.g., SiC, SiO_2, and MnO_2, the contribution of SiO_2 is not considered due to the following reasons. First, the thickness of the SiO_2 layer is very thin. As shown in Fig.3, the thickness ranges from 3 to 8 nm. Second, the effect of SiO_2 layer is to stabilize the interface of SiC whiskers as well as promote the surfactivity of SiO_2 ultrathin layer because SiC is apt to form stable SiO_2 thin layer via adsorbing oxygen even at room temperature.[35]

The pseudocapacitance owing to MnO_2 in the composite is calculated using the following equation:[50]

$$C_{MnO_2} = (C_{SiC/MnO_2} - C_{SiC} \times SiC\%)/MnO_2\%$$

where C_{MnO_2} , C_{SiC/MnO_2} , and C_{SiC} are the specific capacitance of MnO_2, SiC@SiO_2 (NaOH+UV)/MnO_2 and SiC@SiO_2 (NaOH+UV) respectively, and SiC% andMnO_2% are the weight percentages of SiC@SiO_2 (NaOH+UV) and MnO_2 in the composites. By calculation, the specific capacitance of SiC@SiO_2 (NaOH+UV) is 16.6 F g^{-1} at the current density of 0.2 A g^{-1} while the specific capacitance of MnO_2 is to be 395.7 F g^{-1}. It is obvious that pseudocapacitance caused by MnO_2 results in the considerable improvement of supercapacitor properties.

Two primary factors should be responsible for the high capacitance. Firstly, SiC@SiO_2nanocables possess long and straight filament with single crystalline, which contributes to the electron transportation. The structure also provides supporting sites for MnO_2, which further leads to the acceleration of electrons transport. Second, MnO_2 deposited on the surfaces is advantageous to the formation of pores for ion-buffering reservoirs, leading to an efficient redox reaction between MnO_2 and Na^+. What's more, the ions from electrolyte could adequately diffuse and access almost all the available pores of the hybrid electrode when the current density reaches 0.2 A g^{-1}, resulting in a nearly complete intercalation reaction and thus a higher specific capacitance. With the incremental increase of the current density, the effective interaction between the electrode and the ions is reduced significantly, and therefore there is a reduction in specificcapacitance.[51, 52] The mechanism of charge storage of MnO_2 in 1 M Na_2SO_4(aq) may proceed via two reactions as follows.[53] A redox reaction may occur first. Na^+ ions are inserted into and extracted out of the electrode during the reaction as following:

$$MnO_2 + Na^+ + e^- \leftrightarrow MnOONa$$

The second reaction focusing on the adsorption and desorption of Na^+ ions on MnO_2 surface can be expressed as:

$$(MnO_2)_{surface} + Na^+ + e^- \leftrightarrow (MnO_2{}^-Na^+)_{surface}$$

Table1.
Comparison of the capacitance of SiC based supercapacitor electrodes reported in the literature with that in this work

Electrode materials	Capacitance (F g^{-1})	Conditions	Ref.
SiC nanowires	~240 μF cm^{-2}	100 mV s^{-1}	[12]
SiC coated silicon nanowires	~1.7 mF cm^{-2}	50 mV s^{-1}	[13]
SiC nanowires grown on flexible carbon fabric	23 mF cm^{-2}	50 mV s^{-1}	[47]
SiC nanowire film grown on the surface of graphite paper	37 mF cm^{-2}	0.3 A cm^{-2}	[48]
SiC spheres/ nanoneedle MnO_2 composites	273.2 F g^{-1}	10 mVs^{-1}	[49]
SiC spheres	72.4 F g^{-1}	10 mV s^{-1}	[29]
SiC spheres/B-MnO_x	251.3 F g^{-1}	10 mV s^{-1}	[29]
SiC@SiO_2 nanocables	15.3 F g^{-1} =15.0 mF cm^{-2}	0.2 A g^{-1}	In this paper
Modified SiC@SiO_2 nanocables/MnO_2	276.3 F g^{-1} =270.8 mF cm^{-2}	0.2 A g^{-1}	In this paper

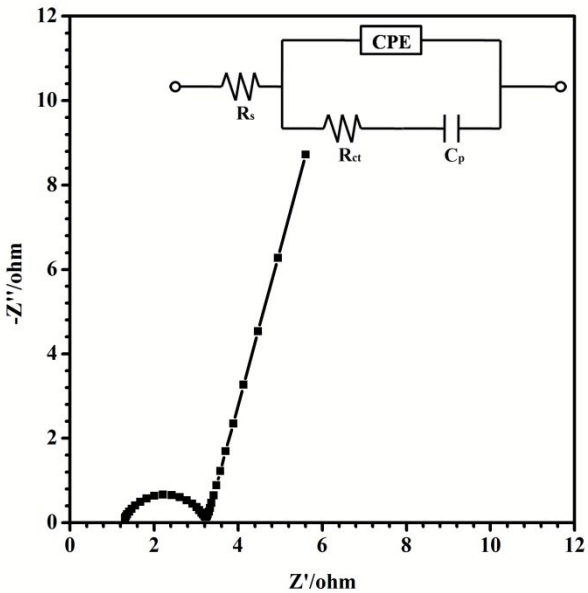

Fig. 9 Nyquist plots of SiC@SiO_2 (NaOH+UV)/MnO_2 electrode. (Inset) Equivalent circuit model.

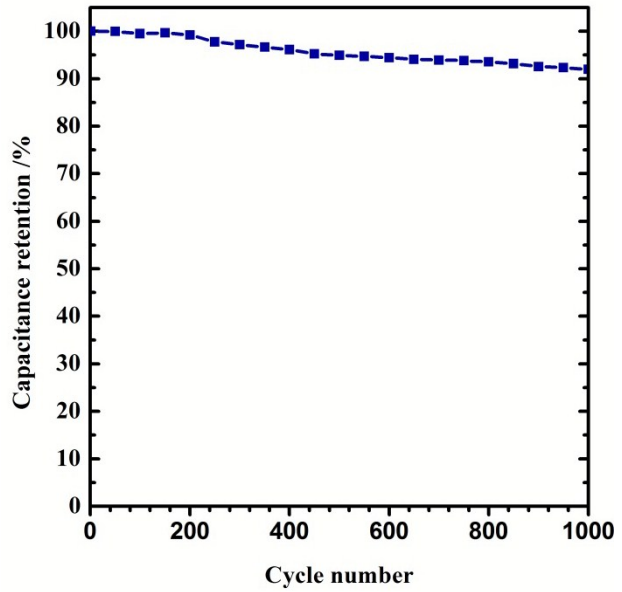

Fig. 10 Cycling stability of SiC@SiO_2 (NaOH+UV)/MnO_2 measured at a scan rate of 10 mV s^{-1}.

Electrochemical impendance spectroscopy (EIS) technique providing important information about the interfacial properties of electrodes is also employed to investigate the conductive and diffusive behavior of SiC@SiO_2 (NaOH+UV)/MnO_2 electrode.[54-56] It is carried out in a frequency range from 0.1 Hz to 100kHz, where Z′ and Z′′ are the real and imaginary parts of the impedance, respectively.(Fig. 9). The Nyquist plot consists of a semicircle in the high-frequency region and a linear part in the low-frequency region. The equivalent circuit diagram (inset in Fig. 9) includes the solution resistance R_s, the charge transfer resistance R_{ct}, a pseudo capacitive element C_p from redox process and the constant phase element (CPE) to account for the double layer capacitance. It is obtained that the linear region of the plot exhibits an angle between 45 and 90° is approximately vertical, which demonstrates an ideal capacitive behavior and low diffusion resistance.[57] In the high-frequency region, R_s and R_{ct} are measured to be 1.26 and 2.01 Ω, respectively. Thus the supercapacitor shows the low charge-transfer resistance and equivalent series resistance with the combinations of low diffusion and electron-transfer resistance responsible for the good electrochemical properties. Furthermore, the result of cycle stability is of the essence as for the electrodes of supercapacitors. In this work, the electrochemically cycling stability of SiC@SiO_2 (NaOH+UV)/MnO_2 electrode is investigated by cyclic voltammetry at the scan rate of 10 mV s^{-1}. As manifested in Fig.10, the capacitance retention for SiC@SiO_2 (NaOH+UV)/MnO_2 electrode attains 91.95% of its original capacitance after 1000 continuous cycles. Based on the above results, it can be concluded that SiC@SiO_2 (NaOH+UV)/MnO_2 electrode (modified SiC@SiO_2 nanocables/MnO_2) exhibits an attractive electrochemical performance.

Conclusions

SiC@SiO_2 core-shell nanocables modified by NaOH solution, UV light irradiation and ultimately deposited by MnO_2 are fabricated to obtain the hybrid electrodes. The results demonstrate that modified SiC@SiO_2 nanocables/MnO_2 possesses a novel encapsulated structure with modified SiC@SiO_2 nanocablesas core and MnO_2 as shell. MnO_2 thin layer in close proximity to the surface of SiC@SiO_2 nanocables results in a tightly connected interface between MnO_2 and nanocables, which promotes the charge transfer and a fast pseudo capacitive reaction. SiC@SiO_2 (NaOH+UV)/MnO_2 electrode exhibits a specific capacitance of 276.3 F g^{-1} at the current density of 0.2 A g^{-1} and long circle life (only 8.05% capacitance loss after 1000 cycles), which is attributed to the synergistic effect of the excellent electrical conductivity, electric double-layer capacity and highly electroactive areas. Our new approach is the combination of modified SiC@SiO_2 nanocables as EDLC materials and MnO_2 as pseudo capacitive material and exhibits the potential application of the hybrid material in supercapacitors and other power source systems.

Acknowledgements

The authors express their appreciation to New Century Excellent Talents in University (NECT-12-0779), the National Science Fund for Excellecnt Young Scholars of China (No. 51522402) and Program for Changjiang Scholars and Innovative Research Team in University (IRT1207) for financial support.

Notes and references

1 A.S. Aricò, P. Bruce, B. Scrosati, J.M. Tarascon and W. Van Schalkwijk, *Nat.Mater.*, 2005, **4**, 366-377.
2 Z. Lei, F. Shi and L. Lu, *ACS. Appl. Mater. Inter.*, 2012, **4**, 1058-1064.
3 S. Bose, T. Kuila, A. K. Mishra, R. Rajasekar, N. H. Kim, and J. H. Lee, *J. Mater. Chem.*, 2012, **3**, 767-784.
4 W. Wei, X. Cui, W. Chen and D.G. Ivey, *Chem. Soc. Rev.*, 2011, **40**, 1697-1721.
5 Z. Cheng, G. Tan, Y. Qiu, B. Guo, F. Cheng, and H. Fan, *J. Mater. Chem. C*, 2015， **3**, 6166-6171.
6 C. Liu, F. Li, L. Ma and H. Cheng, *Adv. Mater.*, 2010, **22**, E28-E62.
7 Z. Lei, N. Christov, L.L. Zhang and X.S. Zhao, *J. Mater. Chem.*, 2011, **21**, 2274-2281.
8 Y. B. Tan and J. Lee, *J. Mater. Chem. A*, 2013, **1**, 14814-14843.
9 Huang, H. and X. Wang, *Nanoscale*, 2011, **3**, 3185-3191.
10 C. Chen, Q. Zhang, X. Zhao, B. Zhang, Q. Kong, M. Yang, Q. Yang, M. Wang, Y. Yang, R. Schlögl and D.S. Su, *J. Mater. Chem.*, 2012, **22**, 14076-14084.
11 J.W. Choi, J. McDonough, S. Jeong, J.S. Yoo, C.K. Chan and Y. Cui, *Nano Lett.*, 2010, **10**, 1409-1413.
12 J.P. Alper, M.S. Kim, M. Vincent, B. Hsia, V. Radmilovic, C. Carraro and R. Maboudian, *J. Power Sources*, 2013, **230**, 298-302.
13 J.P. Alper, M. Vincent, C. Carraro and R. Maboudian, *Appl. Phys. Lett.*, 2012, **100**, 163901-163904.
14 X. Lu, G. Wang, T. Zhai, M. Yu, J. Gan, Y. Tong and Y. Li, *Nano Lett.*, 2012, **12**, 1690-1696.
15 H. Zheng, T. Zhai, M. Yu, S. Xie, C. Liang, W. Zhao, S.C.I. Wang, Z. Zhang and X. Lu, *J. Mater. Chem. C*, 2013, **1**, 225-229.

16 X. Lu, G. Wang, T. Zhai, M. Yu, S. Xie, Y. Ling, C. Liang, Y. Tong and Y. Li, *Nano Lett.*, 2012, **12**, 5376-5381.
17 J. B. Casady and R. W. Johnson, *Solid-State Electron.*, 1996, **39**, 1409-1422.
18 X. Lang, A. Hirata, T. Fujita and M. Chen, *Nat. Nanotechnol.*, 2011, **6**, 232-236.
19 Z. Yu, B. Duong, D. Abbitt and J. Thomas, *Adv. Mater.*,2013, **25**, 3302-3306.
20 X. Li, S. Xiong, J. Li, J. Bai and Y. Qian, *J. Mater. Chem.*, 2012, **22**, 14276-14283.
21 H.A. Pan, O. Ghodbane, Y.T. Weng, H.S. Sheu, J.F. Lee, F. Favier and N.L. Wu, *J. Electrochem. Soc.*, 2015, **162**, A5106-A5114.
22 K. Liang, X. Tang and W. Hu, *J. Mater. Chem.*, 2012, **22**, 11062-11067.
23 S. Cho, K. Shin and J. Jang, *ACS. Appl. Mater. Inter.*, 2013, **5**, 9186-9193.
24 H. Nam, K. M. Kim, S. H. Kim, B. C. Kim, G. G. Wallace and J. M. Ko, *Polym. Bull.*, 2012, **68**, 553-560.
25 R.I. Jafri, A.K. Mishra and S. Ramaprabhu, *J. Mater. Chem.*, 2011, **21**, 17601-17605.
26 H. Chen, T.N. Cong, W. Yang, C. Tan, Y. Li and Y. Ding, *Prog. Nat. Sci.*, 2009, **19**, 291-312.
27 X. Zhang, X. Sun, H. Zhang, D. Zhang and Y. Ma, *Mater. Chem. Phys.*, 2012, **137**, 290-296.
28 L. Gu, Y. Wang, Y. Fang, R. Lu and J. Sha, *J. Power Sources*, 2013, **243**, 648-653.
29 M. Kim and J. Kim, *ACS Appl. Mater. Inter.*, 2014, **6**, 9036-9045.
30 L. Gu, Y. Wang, R. Lu, W. Wang, X. Peng and J. Sha, *J. Power Sources*, 2015, **273**, 479-485.
31 J. Chen, W. Liu, T. Yang, B. Li, J. Su, X. Hou and K. Chou, *Cryst. Growth Des.*, 2014, **14**, 4624-4630.
32 X. Feng and L. Jiang, *Adv. Mater.*, 2006, **18**, 3063–3078.
33 J. Yang, Z. Zhang, X. Men, X. Xu and X. Zhu, *Langmuir*, 2010, **26**, 10198-10202.
34 Y. Huang, X. Chen and M. Q. Zhang, *J. Mater. Sci.*, 2014, **49**, 3025-3033.
35 K. Shimoda, J. Park, T. Hinoki and A. Kohyama, *Appl. Surf. Sci.*, 2007, 253, 9450-9456.
36 J.H. Kim, K.H. Lee, L.J. Overzet and G.S. Lee, *Nano Lett.*, 2012, **11**, 2611-2617.
37 M. Toupin, T. Brousse and D. Bélanger, *Chem. Mater.*, 2002, **14**, 3946-3952.
38 C. D. Wagner, D. E. Passoja, H. F. Hillery, T. G. Kinisky, H. A. Six, W. T. Jansen and J. A. Taylor, *J. Vac. Sci. Technol.*, 1982, **21**, 933-944.
39 Y. Gu, J. Cai, M. He, L. Kang, Z. Lei and Z. Liu, J. Power Sources, 2013, 239, 347-355.
40 G. Li, Z. Feng, Y. Qu, D. Wu, R. Fu and Y. Tong, *Langmuir*, 2004, **26**, 2209-2213.
41 J. Yan, Z. Fan, T. Wei, W. Qian, M. Zhang and F. Wei, *Carbon*, 2010, **239**, 3825-3833.
42 M. Toupin, T. Brousse and D. Bélanger, *Chem. Mater.*, 2004, **16**, 3184-3190.
43 Z. Wu, W. Ren, D. Wang, F. Li, B. Liu and H. Cheng, *ACS Nano*, 2010, **4**, 5835-5842.
44 C. Guo, H. Li, X. Zhang, H. Huo and C. Xu, *Sensor.Actuat. B-Chem.*, 2015, **206**, 407-414.
45 S. Chen, J. Zhu, X. Wu, Q. Han and X. Wang, *ACS Nano*, 2010, **4**, 2822-2830.
46 D. Zhang, X. Zhang, Y. Chen, P. Yu, C. Wang and Y. Ma, *J. Power Sources*, 2011, **196**, 5990-5996.
47 L. Gu, Y. Wang, Y. Fang, R. Lu and J. Sha, *J. Power Sources*, 2013, **243**, 648-653.
48 J. Chen, J. Zhang, M. Wang, L. Gao and Y. Li, *J. Alloy. Compd.*, 2014, **605**, 168-172.
49 M. Kim, Y. Yoo and J. Kim, *J. Power Sources*, 2014, **265**, 214-222.
50 L. Mao, K. Zhang, H. Chan and J. Wu, *J. Mater. Chem.*, 2012, **22**, 1845−1851.
51 Y. Zhang, C. Sun, P. Lu, K. Li, S. Song and D. Xue, *CrystEngComm*, 2012, **14**, 5892−5897.
52 G. Zhu, L. Deng, J. Wang, L. Kang and Z. Liu, *Mater. Res. Bull.* 2012, **47**, 3533−3537.
53 S. Yoon and K. Kim, *Electrochim. Acta.*, 2013, **106**, 135-142.
54 S. Zhong, J. Song, S. Zhang, H. Yao, A. Xu, W. Yao and S. Yu, *J. Phys. Chem. C*, 2008, **112**, 19916-19921.
55 Z. Li, Y. Mi, X. Liu, S. Liu, S. Yang and J. Wang, *J. Mater. Chem.*, 2011, **21**, 14706-14711.
56 J. Wang, Y. Yang, Z. Huang and F. Kang, *Carbon*, 2013, **61**, 190-199.
57 Y. Wang, D. Zhao, Y. Zhao, C. Xu and H. Li, *RSC Adv.*, 2012, **2**, 1074-1082.